

INLET GEOMETRY EFFECT ON COMBUSTION IN A DUCTED ROCKET COMBUSTOR

Tekin Aksu*¹, Can Çıtak¹, Özgür Harputlu¹, M. Tuğrul Akpolat¹ and Ezgi Arısoy¹
Roketsan Missiles Inc.
Ankara, Turkey

ABSTRACT

Reacting Computational Fluid Dynamics (CFD) simulations of a ducted rocket combustor is performed by using chemical equilibrium assumption. Inlet geometry effect on combustion performance is examined. Turbulence – combustion interaction is modeled with PDF functions. Parametric study is held on three different geometry that are 45, 60 and 75 degree inlet entrance angle. Simulations are examined in terms of swirl number and temperature along the combustor. The behavior and decomposition of carbon particles are shown in different inlet geometry angles. Best combustion efficiency, which is in 75 degree inlet geometry angle, has 20 K higher outlet mean temperature. Higher number of swirl enhance fuel air mixing and enhance the decomposition of carbon particles, increase temperature and therefore the efficiency.

INTRODUCTION

Computational fluid dynamics (CFD) simulations of turbulent reacting flows are a great challenge in terms of modeling combustion, turbulence, reaction kinetics and computational power. In addition, the performance of combustion chamber has a great influence of missile performance. Ducted rockets have many advantages when compared with standard rocket engines such as higher specific impulse with longer flight range.

Many groups investigated the combustor performance by means of both experimental and numerical efforts. Liou and Wu (T.-M. Liou, S.-M. Wu, 1988), investigated employing laser-Doppler velocimetry (LDV) measurements in dual-inlet side-dump combustor. Inlet angles are 60 degree and radially position is 180 degree away from each other. Flow characteristics of combustor are discussed. Turbulence intensity on both axial and tangential direction are shown. It is emphasized that the turbulence intensity is diffusive through the downstream of the combustor. In addition, the shape and position of the vortices are described in this study. Moreover, the author implied that the turbulence is highly inhomogeneous and anisotropic just after the air inlet section. Liou and Hwang (T.-M. Liou, Y.-H. Hwang, 1989), performed numerical simulations of a side-inlet ramjet combustor. Inlet geometry angles are 60 degrees for simulations. Results are discussed in terms of swirl intensity, pressure loss and results are

¹ Propulsion Systems Design Department, *corresponding author, email: tekin.aksu@roketan.com.tr

validated with laser-Doppler velocimetry (LDV) data. Ahn and Yoon (K. Ahn, Y. Yoon, 2006), examined model side-dump combustor for different inlet geometry angles with particle image velocimetry (PIV). Inlet geometry angles are 45, 60 and 90 degree for experimental configurations. Experiments are discussed in terms of mean velocity vectors and longitudinal components of the centerline velocities. The height of recirculation zone is maximum in 90-degree inlet angle geometry; however, the length of recirculation zone is maximum at 60 degree inlet angle. Liou and Liao (Tong-Miin Liou, Chin-Chun Liao, 1995), studied on a guide vane on inlet combustor section. Experimental studies are conducted with LDV measurement technique. Guide vane diminish the effect of inlet flow distortions and reduce the velocity differences on outer and inner wall at the inlet section. Secondary flow is stronger and flow is uniform when compared with no guide vane measurements. Therefore, guide vane can enhance the overall combustor performance.

Thangadurai et al. (G. Raja Singh Thangadurai, B. S. Subhash Chandran, V. Babu, T. Sundararajan, 2004; G. Raja Singh Thangadurai, B. S. Subhash Chandran, V. Babu, T. Sundararajan, 2006), performed two different studies, which are the inlet angle and the air-fuel ratio effects of the ramjet combustor performance. Three different inlet angles, 30, 45 and 60-degree, are compared with chemical equilibrium approach by using standard $k-\epsilon$ turbulence model. Also, turbulence-chemistry interaction is modeled with probability density functions (PDF). Fuel is surrogated as kerosene and particle diameter is $20 \mu\text{m}$. Particles are modeled with Lagrangian approach. When effect of air inlet angle examined, higher temperature at the combustor outlet is obtained in 60-degree inlet angle. The combustion performance of 60 degree inlet angle is 14 percent higher than 30 degree inlet angle. An important point is investigated when the effect of air-fuel ratio simulations are conducted. Air fuel ratio of 10 and 30 simulations have identical outlet mean temperatures. Therefore, it can be said that the fuel-air mixing is not sufficient for 10 air-fuel ratio configurations. Air momentum is not sufficient for mixing and ideal combustor performance. In order to assess the combustor performance, Hewitt (Hewitt, 2008), conducted a series of simulations and experimental studies. Boron fuel properties are solved on gas generator by using 0-D chemical equilibrium solver. Due to modeling problems and complexities in boron combustion, boron particles are surrogated as fixed carbon particles. Combustion is modeled with chemical equilibrium assumption with PDF functions. Carbon particles are presented as $20 \mu\text{m}$. Radiation effects are also modeled with P1 radiation model. Kim and Natan (Soojong Kim and Benveniste Natan, 2015), examine the inlet positions and equivalence ratio effects on ducted rocket combustor. Three different inlet positions are compared that are 4 inlet 90-degree, 2 inlet 180-degree and 2 inlet 90 degree. Inlet entrance angle is fixed for all simulations, which are 60 degrees. Chemical equilibrium effects with PDF approach is used with P1 radiation model. Moreover, combustor equivalence ratios of 0.35, 0.64 and 0.98 are examined. Particle mass trajectories are presented with combustor longitudinal temperature distribution is discussed for all simulations. The effect of inlet performance is negligible at lower equivalence ratios. However, higher equivalence ratios inlet positions are great effect and influence on combustor performance. Also, numerical model is validated with experimental efforts.

METHODOLOGY

In order to assess the performance effects of combustion chamber entrance geometry and fuel – air mixing, reactive CFD simulations are performed. Three different inlet geometry models that are 45 degree, 60 degree and 75 degree, are compared in terms of temperature, gas phase fuel mixture fraction, solid carbon mixture fraction and swirl number. Combustor illustration is shown in Figure 1.

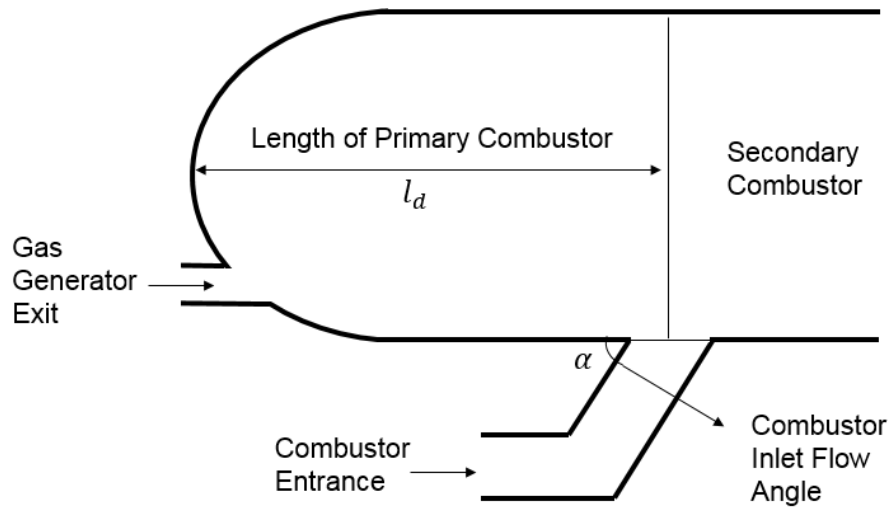


Figure 1: Combustion Chamber Illustration

Combustion chamber fuel-air mixing takes key role in combustion efficiency. Turbulence in ducted ramjet combustion chamber is modeled with Realizable $k-\varepsilon$ turbulence model and combustion is modeled with the probability density function approach with a chemical equilibrium assumption (Thierry Poinso, 2005). Turbulence-chemistry interaction is presumed as β -function shape. Fuel stream is examined with two different streams, one for gas phase and other for solid phase. Main advantage for chemical equilibrium assumption that model does not require any Arrhenius rate or coefficients. Particle injection is performed with Lagrangian approach. Particles are emphasized as $10 \mu\text{m}$. Fuel, used for numerical simulations, is glycidyl azide polymer (GAP) and carbon mixture. Fuel composition of GAP/carbon is used from Kim and Natan (Soojong Kim and Benveniste Natan, 2015), which GAP's products that is solved from CEA thermo-equilibrium solver. Fuel composition is shown in Table 1.

Table 1: GAP/Carbon fuel composition.

GAP/carbon		
	Temperature, K	1250
Mole fraction	CH4	0.012
	CO	0.128
	H2	0.315
	H2O	0.006
	N2	0.206
	C(graphite)	0.331
	others	0.002
	Total	1.0

Favre averaged flow equations are shown below.

$$\frac{\partial \bar{\rho}}{\partial t} + \frac{\partial}{\partial x_i} (\bar{\rho} \tilde{u}_i) = 0 \quad (1)$$

$$\frac{\partial(\overline{\rho\tilde{u}_i})}{\partial t} + \frac{\partial}{\partial x_i}(\overline{\rho\tilde{u}_j\tilde{u}_i}) = -\frac{\partial\overline{p}}{\partial x_i} + \frac{\partial}{\partial x_j}(\overline{\tau_{ij}} + \overline{\rho u_j'' u_i''}) \quad (2)$$

$$\frac{\partial(\overline{\rho\tilde{H}})}{\partial t} + \frac{\partial}{\partial x_j}(\overline{\rho\tilde{u}_j\tilde{H}}) = -\frac{\partial}{\partial x_j}(\overline{\rho\alpha} \frac{\partial\tilde{H}}{\partial x_j} + \overline{\rho u_j'' H''}) + \overline{S_H} \quad (3)$$

In order to resolve turbulence Favre averaged flow equations are solved and turbulence related $\overline{\rho u_j'' u_i''}$, $\overline{\rho u_j'' H''}$ ve $\overline{\rho u_j'' Y_m''}$ terms need to be modeled. Reynolds stress tensor is defined with Boussinesq approach. According to this approach Reynolds stress tensor is implied as equation 4.

$$\overline{\rho u_j'' u_i''} = \mu_t \left(\frac{\partial\tilde{u}_i}{\partial x_j} + \frac{\partial\tilde{u}_j}{\partial x_i} \right) - \frac{2}{3} \mu_t \frac{\partial\tilde{u}_k}{\partial x_k} \delta_{ij} - \frac{2}{3} \overline{\rho k} \delta_{ij} \quad (4)$$

Other two terms are defined as in equation 5 and 6.

$$\overline{\rho u_j'' H''} = \frac{\mu_t}{Pr_t} \frac{\partial\tilde{H}}{\partial x_j} \quad (5)$$

$$\overline{\rho u_j'' Y_m''} = \frac{\mu_t}{Sc_t} \frac{\partial\tilde{Y}_m}{\partial x_j} \quad (6)$$

Realizable k - ε turbulence (Shih, T. H., Liou, W. W., Shabbir, A., Yang, Z., Zhu, J., 1995) turbulence kinetic energy and dissipation rate is transported as shown in equation 7 and 8.

$$\frac{\partial(\overline{\rho k})}{\partial t} + \frac{\partial(\overline{\rho\tilde{u}_j k})}{\partial x_j} = \frac{\partial}{\partial x_j} \left(\left(\mu + \frac{\mu_t}{\sigma_k} \right) \frac{\partial k}{\partial x_j} \right) + P - \overline{\rho\varepsilon} \quad (7)$$

$$\frac{\partial(\overline{\rho\varepsilon})}{\partial t} + \frac{\partial(\overline{\rho\tilde{u}_j\varepsilon})}{\partial x_j} = \frac{\partial}{\partial x_j} \left(\left(\mu + \frac{\mu_t}{\sigma_\varepsilon} \right) \frac{\partial\varepsilon}{\partial x_j} \right) + C_{\varepsilon 1} \frac{\varepsilon}{k} P - C_{\varepsilon 2} \overline{\rho} \frac{\varepsilon^2}{k} \quad (8)$$

Computational grid consists 7 million polyhedral mesh with structural wall layer mesh. Computational grid is shown in Figure 2. In simulations, fuel mass flow rate is 80 g/s and air/fuel ratio is 15. Air inlet temperature is 420 K.

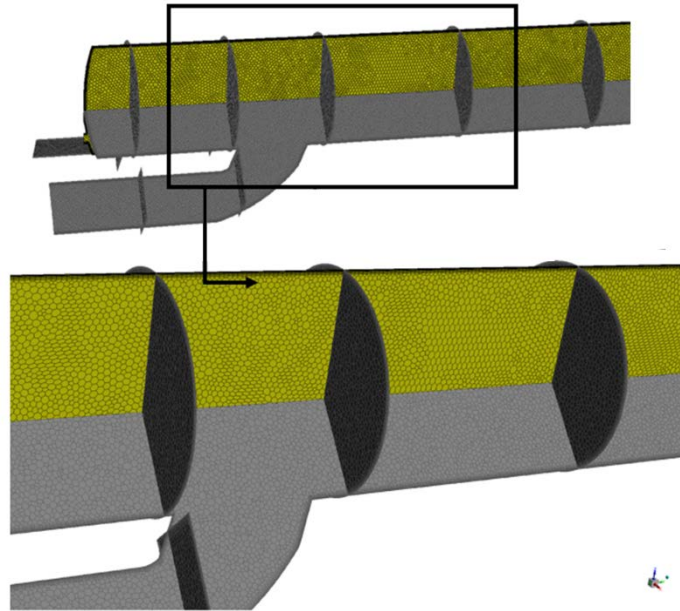


Figure 2. Computational Grid Representation.

RESULTS

Mach number distribution for different inlet geometry angles is presented in Figure 3. 60 and 75 degree inlet angle has flow separations at the entrance elbow. These two configurations have similar behavior at primary combustor section. However, downstream inlet angle effects are diminished and all configurations have almost same velocity profile by 5% at combustor outlet plane.

Temperature distribution for different inlet geometry angles is presented in Figure 4. It is expected that swirl number and primary combustor mixing increase while inlet geometry angle increase. As expected, temperature of primary combustor, is higher in 75 degree and 60 degree combustor inlet angle because recirculation zone has more momentum for these two configurations.

Temperature distribution along the combustor is shown in Figure 5. Primary combustor temperatures vary from each other because of fuel-air mixing differences. Fuel air mixing is inadequate in 45 degree air inlet configuration. Gas temperature of the fuel is forced as 1250 K, however fuel-air mixing at that configuration only sustain 1000 K. Therefore, it can be said that gas phase reactions are not started. For 60 and 75 degree configurations, fuel-air mixing is started and peak temperature at that section is around 1400 K. Gas phase reactions play important role in ignition and burning of solid particles. At secondary combustor, solid particles are started to ignite and burn. Zoomed view of outlet temperature section is shown in Figure 6.

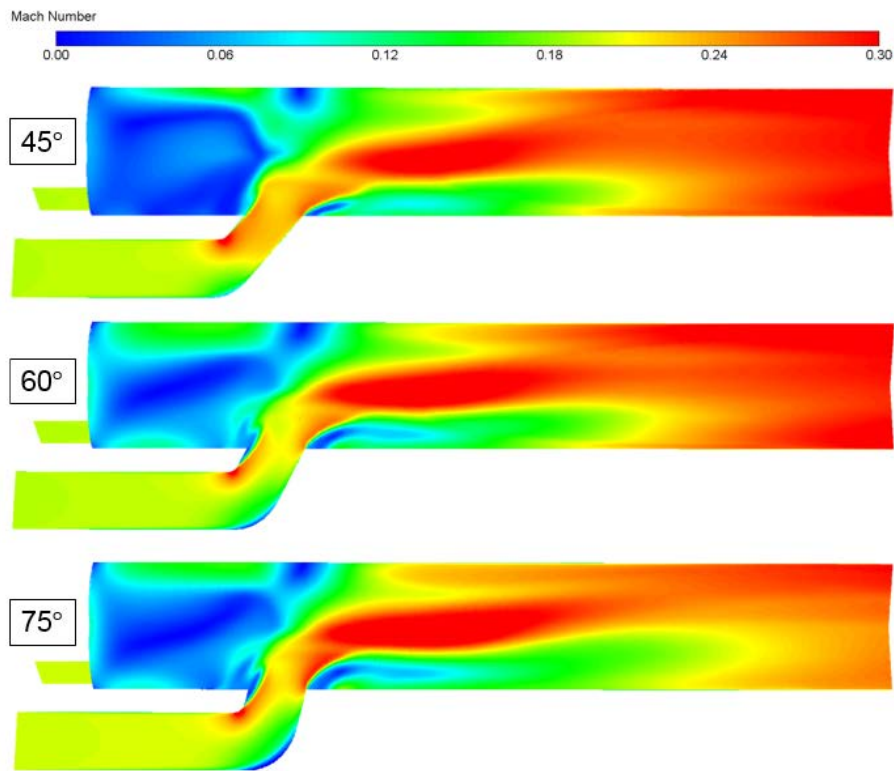


Figure 3: Combustion Chamber Mach Number Distribution for Different Inlet Geometry Angles

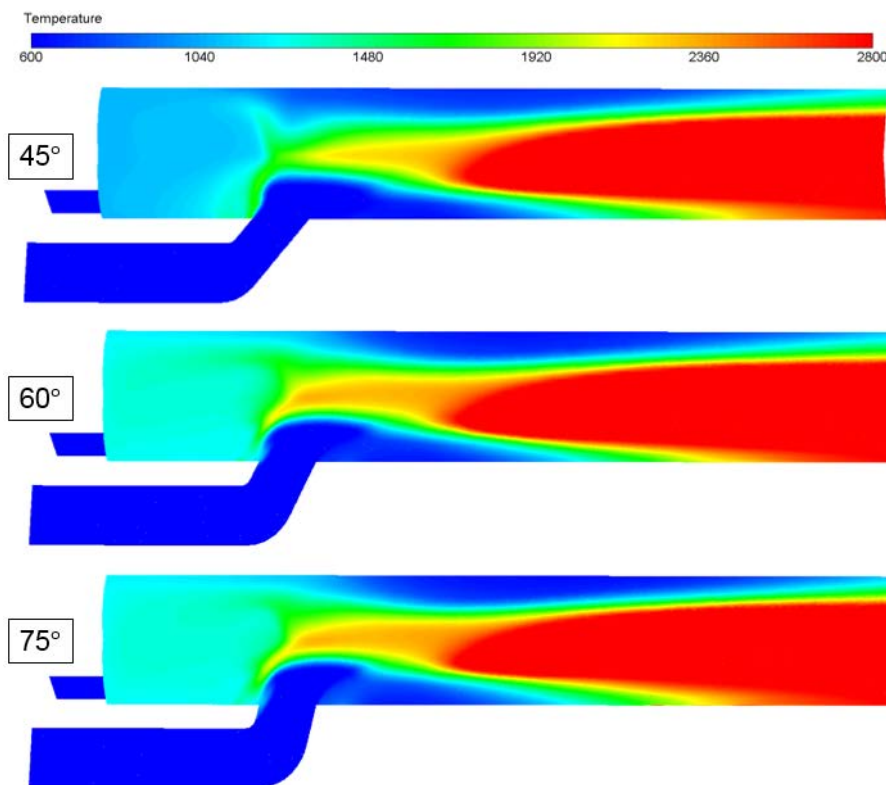


Figure 4: Combustion Chamber Temperature Distribution for Different Inlet Geometry Angles

As expected, 75 degree inlet angle has higher temperature than 45 and 60 degree inlet angle. Inlet angle of 75 degree has 25 K higher outlet mean temperature when compared with 45 degree inlet angle. In addition, 60 degree inlet angle has 15 K higher temperature when compared with 45 degree inlet angle.

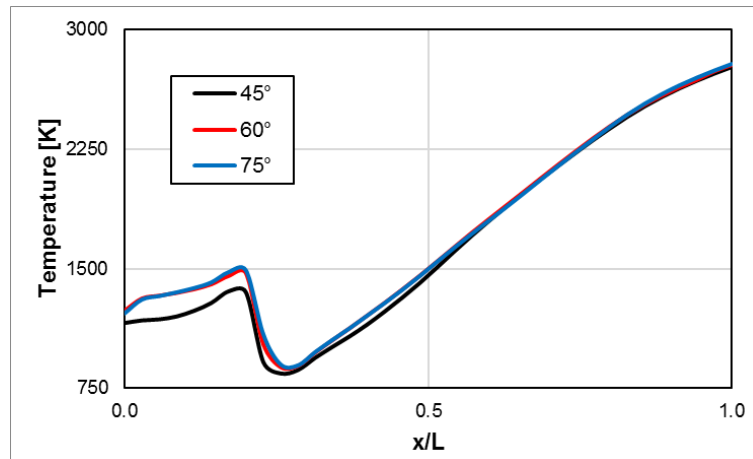


Figure 5: Mean Temperature of Combustor for Different Inlet Geometry Angles

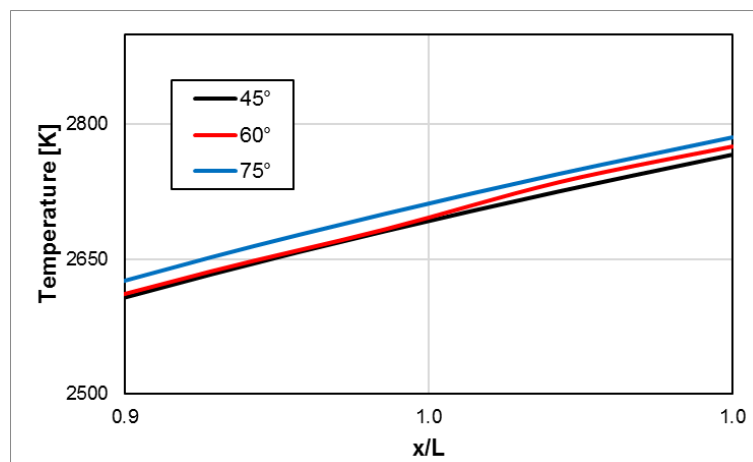


Figure 6: Mean Temperature of Combustor for Different Inlet Geometry Angles (Zoomed View at Outlet Part)

Combustion chamber temperature distributions at combustor cross sections are shown in Figure 7 with respect to different inlet angle geometries. At 45 degree inlet angle combustion chamber it is shown that primary zone of the combustor's temperature increase is lower than other two configurations. Temperature at primary zone is similar for 60 and 75 degree inlet angle. Moreover, the turbulence is anisotropic and non-homogeneous at combustor differences are observed in temperature distribution.

In addition, gas phase fuel mixture fraction of combustor for different inlet geometry angles are shown in Figure 8. That figure means, the gas phase fuel is consumed, after air inlet is included in combustor suddenly in primary zone, all the gas phase is consumed.

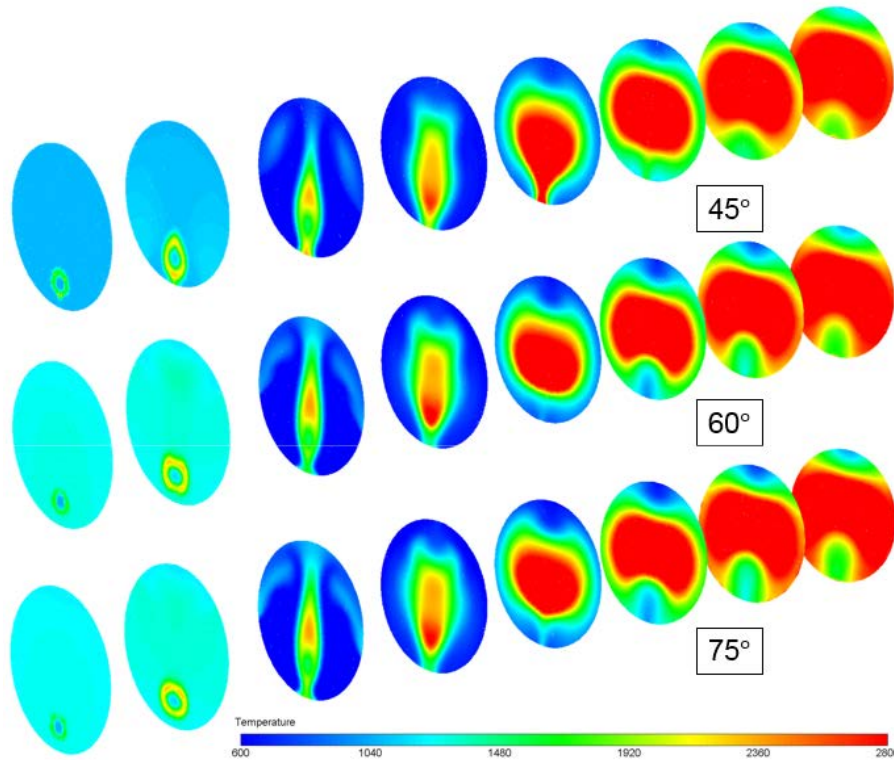


Figure 7: Combustion Chamber Temperature Distribution for Different Inlet Geometry Angles at Cross Section Planes

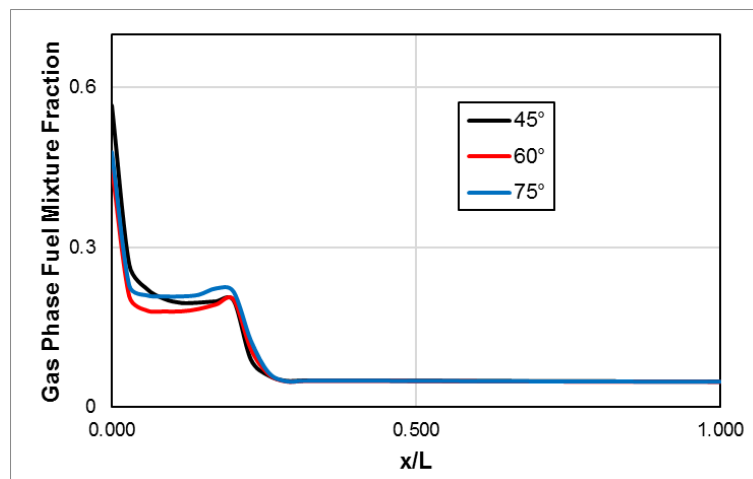


Figure 8: Gas Phase Fuel Mixture Fraction of Combustor for Different Inlet Geometry Angles

Combustion chamber carbon particle mass streamlines are presented in Figure 9. The behavior of streamlines are similar for all configurations. Carbon particle streams diffused constantly. From that information the momentum of fuel stream is strong and the momentum of air stream is weak when compared with fuel stream. For lower equivalence ratios combustor performance will be higher. Solid carbon mixture fraction of combustor for different inlet geometry angles are shown in Figure 10. Solid phase is diminished by airflow stream. Zoomed view of solid carbon mixture fraction is presented in Figure 11. Higher swirl decompose higher carbon fraction as shown in figure. Higher carbon decomposition provides higher temperatures. These data are completely compatible with temperature plots.

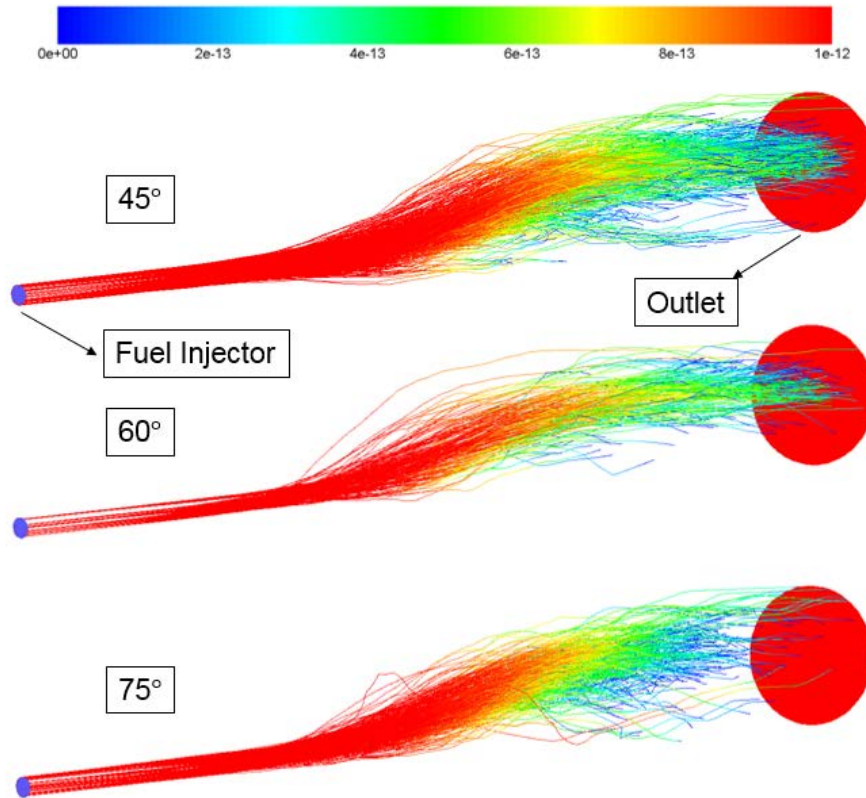


Figure 9: Combustion Chamber Carbon Particle Mass Streamlines

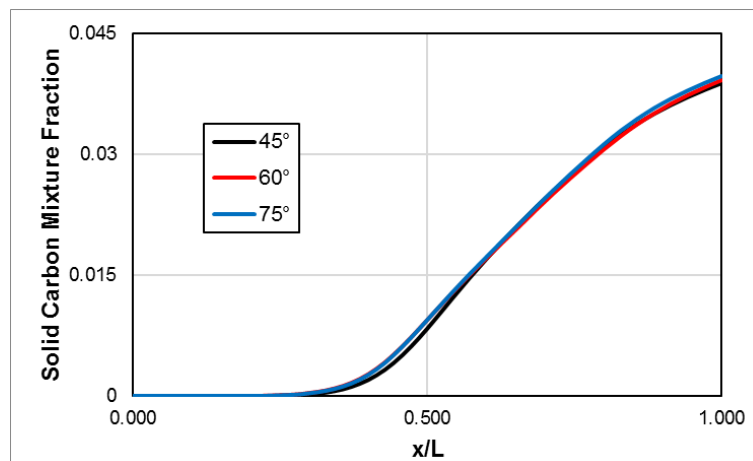


Figure 10: Solid Carbon Mixture Fraction of Combustor for Different Inlet Geometry Angles

Swirl number for ducted rocket combustor is shown in Figure 12. Maximum swirl number is at 75 degree inlet angle. All data is normalized with 75 degree inlet angle swirl number. Last but not least, the swirl number depict the decomposition of carbon particles. Higher carbon particle fraction, increase the temperature and thereby the efficiency. Swirl number is increased when air flow momentum included the combustion chamber and diffuse along the outlet of the combustor.

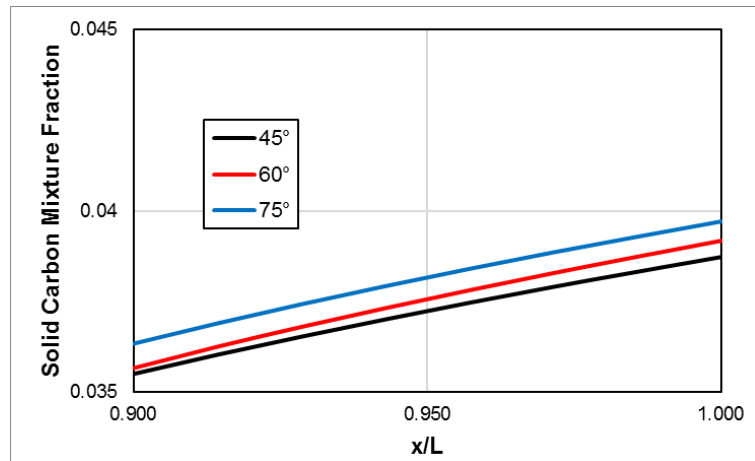


Figure 11: Solid Carbon Mixture Fraction of Combustor for Different Inlet Geometry Angles (Zoomed View at Outlet Part)

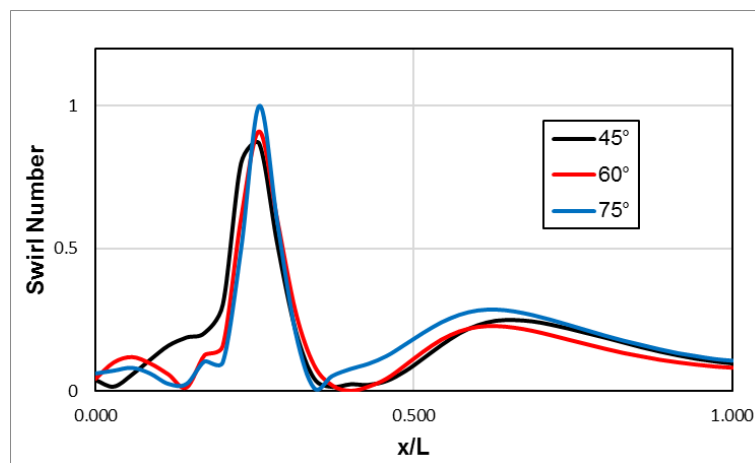


Figure 12: Swirl Number of Combustor for Different Inlet Geometry Angles

CONCLUSION

In conclusion, numerical analysis of ducted rocket combustor at different inlet geometry angles are performed and are discussed in terms of swirl number and combustion efficiency. At primary combustor region, gas phase fuel is consumed. Thus, temperature increase along the downstream of the combustor is observed. With increasing temperature, solid carbon starts burning. Swirl number is higher in 75 degree inlet combustor angle. That affect the momentum in primary of combustor. This implies that the flow structure influenced solid carbon particles and higher combustor outlet temperature

FUTURE WORK

For future studies, different fuel-air ratio simulations will be performed with different primary combustor lengths.

REFERENCES

- G. Raja Singh Thangadurai, B. S. Subhash Chandran, V. Babu, T. Sundararajan. (2004). Numerical Investigation on Effect of Inlet Dump Angle on Ramjet Combustor Performance. *40th AIAA/ASME/SAE/ASEE Joint Propulsion Conference and Exhibit*. Fort Lauderdale, Florida.
- G. Raja Singh Thangadurai, B. S. Subhash Chandran, V. Babu, T. Sundararajan. (2006). Numerical Investigation on Effect of Air/Fuel Ratio on Ramjet Dump Combustor Performance. *42nd AIAA/ASME/SAE/ASEE Joint Propulsion Conference & Exhibit*. Sacramento, California.
- Hewitt, P. W. (2008). *Numerical Modeling of a Ducted Rocket Combustor With Experimental Validation*. Blacksburg, Virginia: University of Virginia, PhD Dissertation.
- K. Ahn, Y. Yoon. (2006). Characterization of Side-Dump Combustor Flowfield Using Particle Image Velocimetry. *Journal of Propulsion and Power*, 22(3), 527-533.
- Shih, T. H., Liou, W. W., Shabbir, A., Yang, Z., Zhu, J. (1995). A New k- ϵ Eddy Viscosity Model for High Reynolds Number Turbulent Flows. *Computers Fluids*, 24(3), 227-238.
- Soojong Kim and Benveniste Natan. (2015). Inlet Geometry and Equivalence Ratio Effects on Combustion in a Ducted Rocket. *Journal of Propulsion and Power*, 31(2), 619-631.
- T.-M. Liou, Y.-H. Hwang. (1989). Calculation of Flowfields in Side-Inlet Ramjet Combustors with an Algebraic Reynolds Stress Model. *AIAA Journal of Propulsion*, 5(6), 686-693.
- Thierry Poinso, D. V. (2005). *Theoretical and Numerical Combustion*. R.T. Edwards, Inc.
- T.-M. Liou, S.-M. Wu. (1988). Flowfield in a Dual-Inlet Side-Dump Combustor. *AIAA Journal of Propulsion*, 4(1), 53-60.
- Tong-Miin Liou, Chin-Chun Liao. (1995). Flows in a Curved Combustor Inlet with and Without a Guide Vane. *Journal of Propulsion and Power*, 11(3), 464-472.